

Remote Sensing Monitoring System of Land Coverage Change in Mining Area

¹ Yanbin WU, ² Liangjun LI

¹ School of Management Science and Engineering, Hebei University of Economic and Business,
Shijiazhuang 050061, China

² Public Geological Survey Management Center of Anhui Province,
Hefei 230001, China
E-mail: yanbin_wu@yeah.net

Received: 20 September 2013 /Accepted: 25 October 2013 /Published: 30 November 2013

Abstract: Based on remote sensing images, the panoramic views of land coverage distribution across a large geographic area can be accessed conveniently. Remote sensing monitoring system of land coverage change in mining area, which is a complex information system based on spatial database to manage multi-source heterogeneous data, was proposed in this article. The system structure, function and development strategy were studied in this paper. Remote sensing image fusion and classification are the key technologies in this system. The remote sensing image fusion method which is based on multi-band wavelet was discussed. Based on remote sensing image, the Chaos Immune Algorithm was proposed to improve the accuracy of land coverage classification. The results showed that this system can integrate the multi-source heterogeneous spatial data, including remote sensing image, vector data and related properties data into the whole body, also demonstrate graphical visualization and analyze compositely. Copyright © 2013 IFSA.

Keywords: Remote sensing images, Monitoring system, Land coverage change, Mine area, Fusion, Classification.

1. Introduction

Mining activity is the most important factor which causes the land coverage change in the mining area. The Remote Sensing (RS) data can do the task of monitoring a large range area in the mining area, reflecting the panorama distribution information of continuous land and space coverage change visually. RS technology has many advantages, including macro, objective, comprehensive, dynamic, speedy, etc., providing a scientific basis for carrying out land reclamation & management and surface ecological restoration & reconstruction in the mining area. RS monitoring system of land coverage change in mining

area is a system which can research and develop on the basis of RS survey results in the mining subsidence. It mainly integrates and analyzes RS images from different sensors and multi-temporal data as well as does the job of processing graphics and image through combination analyzing of surface and image data [1].

2. System Overall Design

RS survey of land coverage in the mining area mainly takes advantage of satellite sensing images from different period of time and makes comparative

analysis of these images in order to explain the plane continuous distribution and development of land coverage from different periods. It achieves effective integration and unified management of multiple heterogeneous data sources, including multiple RS satellite data, ground-truth data, vector data, property data, etc., and established a characteristic professional RS image processing system which has functions of image processing & analysis and data management & query [2]. It adopts modular function and multilevel open architecture as its design structure to fulfill the implementation of system software development. Based on the above analysis, the system frame is as Fig. 1.

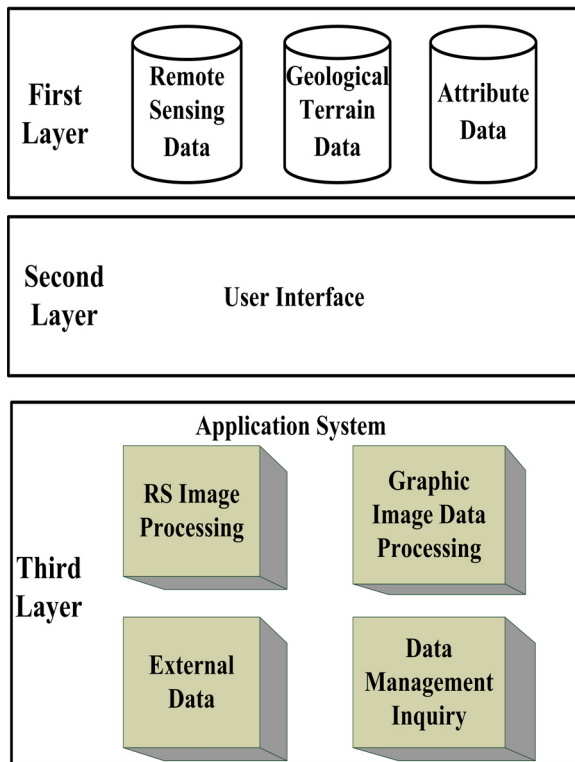


Fig. 1. System development frame diagram.

Foreground program of the system was developed by the fourth-generation matrix programming language IDL, and SQL Server2010 and Oracle10G was supported in backend database. The object-oriented spatial data and attribute data were stored integratively through the relational database. Through SQL Server2010 or Oracle10G, the space and attribute data were stored as concentrated or distributed multi-source data. The DirectX9.0C was used to be the 3D graphics engine. MapX combining SpatialWare provided by MapInfo was adopted to be the spatial database engine for the server data processing. So the development of high flexibility and system scalability is more advantageous to the people of the cooperative development and system of effective seamless integration.

3. Key Technology

Remote sensing image fusion can decrease the incompleteness, multiplicity, and uncertainty which probably exists in interpreting target objects [3]. So, it can greatly improve the effectiveness in feature extraction, classification, and target recognition. Remote sensing image fusion is an important part of remote sensing technology, and it is a major means for intensifying the remote sensing information [4]. By using the multi-ary wavelet transform model which combined with multiple texture information, this system completes the image fusion with different resolution ratio.

Remote sensing image classification is the most important part in quantitatively obtaining land cover changes in mining area. To improve the image classification accuracy, Chaos Immune Algorithm was adopted in this system.

3.1. Remote Sensing Image Fusion

The remote sensing image fusion method based on multi-band wavelet was applied in this system. The orthogonal decomposition in the square integrable function space $L^2(R)$ can be acquired based on multi-scale analysis theory [5, 6].

If $V_{j+1} = W_j^s \oplus V_j$ ($1 \leq s \leq M-1$), $j \in Z$, then for every integer N and $M > 0$, the following formula holds:

$$V_N = W_{N-1}^s \oplus W_{N-2}^s \oplus \dots \oplus W_{N-M}^s \oplus V_{N-M}, \quad (1)$$

where W_j^s , V_j are the closed subspace columns.

The closed subspace column V_j is generated from $\left\{ \varphi_{j,k} = M^{\frac{j}{2}} \varphi(M^j x - k) \mid K \in Z \right\}$, which is the orthogonal basis, while W_j is generated from $\left\{ \psi_{j,k}^s = M^{\frac{j}{2}} \psi_{j,k}^s(M^j x - k) \mid 1 \leq s \leq M-1, K \in Z \right\}$, where $\varphi(x)$ is the scale function, and $\left\{ \psi^s(x) \mid 1 \leq s \leq M-1 \right\}$ called the wavelet function which satisfies the following equations:

$$\begin{cases} \varphi(x) = \sum_{k \in Z} c_k \varphi(Mx - k) \\ \psi^s(x) = \sum_{k \in Z} d_k^s \varphi(Mx - k) \end{cases}, \quad (2)$$

where $\varphi(x)$ is the scale function and $\psi^s(x)$ is wavelet function. Where c_k is the filtering coefficient and d_k^s is the wavelet coefficient, there is an orthogonality relationship between them. And the filtering equation is:

$$H(z) = \frac{1}{M} \sum_{k \in z} c_k z^k \quad (3)$$

The multi-ary wavelet was applied to decompose the 2-D energy-limited signal $f^2(x, y) \in L^2(R)$ of remote sensing images:

$$\begin{aligned} a_{j+1,k,l} &= \sum_m \sum_n c_{m-Mk} c_{n-Ml} a_{j,m,n} \\ b_{j+1,k,l}^{t,s} &= \begin{cases} \sum_m \sum_n c_{m-Mk} d_{n-Ml}^s a_{j+1,m,n} & t=0, 1 \leq s \leq M-1 \\ \sum_m \sum_n d_{m-Mk}^t c_{n-Ml} a_{j+1,m,n} & 1 \leq t \leq M-1 \\ \sum_m \sum_n d_{m-Mk}^t d_{n-Ml}^s a_{j+1,m,n} & t \geq 1, M-1 \geq s \end{cases} \end{aligned} \quad (4)$$

where $j = 0, 1, 2, \dots$, $\{a_{j,k,l}\}$ is the low frequency component of the j -th layer decomposed and $\{b_{j,k,l}^{t,s}\}$ the high frequency component of the j -th layer decomposed. M -ary wavelet decomposition may generate one low frequency component and $M^2 - 1$ high frequency component. The reconstructed equation is:

$$\begin{aligned} C_{j,k,l} &= \sum_m \sum_n c_{k-Mm} c_{l-Mn} a_{j+1,m,n} \\ &+ \sum_{t,s=0, s+t \neq 0}^{M-1} \sum_m \sum_n d_{k-Mm}^t d_{l-Mn}^s b_{j+1,m,n}^{t,s} \end{aligned} \quad (5)$$

3.2. Remote Sensing Image Classification

The core of Chaos Immune Algorithm is based on the biologic immune mechanism reflected in mathematics the embodiment of biological immune mechanism in mathematics. Combining with random-choice and determinacy, Artificial Immune Algorithm is a heuristic random searching algorithm which has the ability to develop [7, 8].

Ag was defined initial antigen and Ab was defined initial antibody populations. M denoted the scale of antibody populations. $X_m = \{x_{m1}, x_{m2}, \dots, x_{mi}, \dots, x_{mn}\}$ denoted an initial antibody, $m = 1, 2, \dots, M$ $i = 1, 2, \dots, n$. n was the dimension of variable X_m . Similar with genetic algorithm, x_{mi} was called allele, $x_{mi} \in [a_{mi}, b_{mi}]$. Antibody bit string was divided into l segments and every segment length was n_i , so, $n = \sum_{i=1}^l n_i$ denoted total length of antibody gene segment. $Y(0) = (y_{0,1}, y_{0,2}, \dots, y_{0,i})$ ($i = 1, 2, \dots, n$) was defined initial antibody populations center. After k iterations, the Euclidean distance reciprocal between individual and antibody populations center was defined affinity function:

$$\frac{1}{aff(X_m)} = \left(\sum_{i=1}^n |x_{mi} - y_{ki}|^2 \right)^{\frac{1}{2}} \quad (6)$$

$$m = 1, 2, \dots, M \quad i = 1, 2, \dots, n$$

Main operators as follows:

1) Chaos optimization of initial population.

The initial Ab were optimized through chaos operator. According to equation (7) a chaotic-type initial value γ_{mi}^0 was produced [8].

$$\gamma_{mi}^0 = (x_{mi} - a_{mi}) / (b_{mi} - a_{mi}) \quad (7)$$

$$m = 1, 2, \dots, M \quad i = 1, 2, \dots, n$$

The logistic map was used to generate chaotic variable γ_i^k .

$$\gamma_i^{k+1} = \mu \gamma_i^k (1 - \gamma_i^k) \quad , \quad (8)$$

$$i = 1, 2, \dots, n \quad k = 0, 1, 2, \dots$$

where μ was the control parameter, after determined the value of μ , with the arbitrary initial value $\gamma_i^0 \in (0, 1)$ (except 0.25, 0.5, 0.75 the fixed point of equation(8)), an assured time series $\gamma_i^1, \gamma_i^2, \dots, \gamma_i^k$ can be iterated [8].

Chaos optimization algorithm is mapping the chaos space to the solution space, using the inherent properties of chaotic variables to fulfill the overall search. According to equation (9), map the chaos variables from chaos space to the solution space [8].

$$x_{mi} = a_{mi} + (b_{mi} - a_{mi}) \gamma_{mi}^k \quad (9)$$

$$m = 1, 2, \dots, M \quad i = 1, 2, \dots, n$$

Set x_{mi}^* as the optimal solution at the current phase of coarse-grained search, aff^* is the optimal objective function value for current phase. After each iteration, the individual affinity function $aff(k)$ was calculated, iteration termination condition was $aff(k) \leq aff^*$. The antibody population after optimization was denoted by Ab' .

2) Clone selection operator.

After the combination of antibody with antigen, antigen can be destroyed through a series of reactions which are based on antibody concentration. Antibody concentration $d(X_m)$ was defined by the following expression.

$$d(X_m) = \left[\frac{1}{M} \sum_{q=1}^M \frac{1}{1 + \sqrt{\sum_{i=1}^n (x_{mi} - x_{qi})^2}} \right]^{\alpha \cdot \left(\frac{1-g}{G} \right)} \quad , \quad (10)$$

where α is the system parameter to adjust algorithm convergence speed, g is the current evolution generation and G is the maximum evolution generation.

Affinity function $aff(X_m)$ was adjusted through the following expression. After the adjustment, $aff(X_m)$ was denoted by $\tilde{aff}(X_m)$.

$$\tilde{aff}(X_m) = aff(X_m)/d(X_m) \quad (11)$$

These antibodies which have bigger individual affinity value and the lower concentration can be promoted, on the contrary, those antibodies with smaller individual affinity value and the higher concentration can be inhibited, thus this process ensured the diversity of antibody group, so as to escape from local optima.

3) Clone operator

According to \tilde{aff} , antibodies in Ab' were ordered by sort descending. Take top m_c antibodies to be cloned, the antibody group cloned was denoted by Ab_c . As the following equation, the population size of Ab_c can be calculated [9, 10].

$$M_c = \sum_{j=1}^{m_c} \text{round}\left(\frac{\beta M}{j}\right), \quad (12)$$

where M_c is the population size of Ab_c . β is the proliferation coefficient to control antibody group size owing to its influence of algorithm iteration and calculating time. j is the sequence number of antibody by sort descending. $\text{round}(\cdot)$ is the rounding operation.

4) Variation Operator.

Set $\bar{X} = (\bar{x}_1, \dots, \bar{x}_{i-1}, \bar{x}_i, \dots, \bar{x}_n)$ as a parent entity, according to equation (13) to mutate, then after the Variation, the offspring individual was \tilde{X}_m , the antibody group mutated was denoted by Ab_m .

$$\tilde{X}_m = \bar{X}_m + \eta N(0,1)e^{-\tilde{aff}} \quad (13)$$

After (0,1) standardization, aff of \bar{X}_m was denoted by \tilde{aff} . $N(0,1)$ was normal random function with mean value $\mu=0$ and variance $\sigma=1$. The proportionality constant η can control attenuation of negative exponential function. According to equation (13), the bigger the antibody affinity value, the smaller variation, that was beneficial to maintain the stability of the local optimal solution.

5) Excellent individual chaotic disturbance.

After the clone selection, clone and variation, we get the current optimal solution is $X^* = (x_1^*, \dots, x_{i-1}^*, x_i^*, \dots, x_n^*)$, according to equation (14), make chaotic disturbances to x_i^* .

$$x_i(k') = x_i^* + \varphi u_{k,i} \quad i = 1, 2, \dots, n \quad (14)$$

In the equation, $x_i(k')$ is the chaotic variable of a smaller range of ergodicity relative to equation (8), φ is the adjustment coefficient related to the iteration number k' , in this paper set $\varphi = 1 - \left(\frac{k'-1}{k'}\right)^n$.

Continue to carry out iterative search with $x_i(k')$, the termination condition is $aff(k') \leq aff^*$.

4. System Simulation

The following figures are the simulation results of this system. Huainan mine in Anhui Province was selected as the case of target area. TM and SPOT remote sensing images are the main experiment image data. Fig. 2 is the original TM 2, 3, and 4 images of 2004 in Kongji coal mine-Bagongshan-Caijiagang area and Fig. 3 is SPOT-PAN of 2004 with a resolution of 10 m. Fig. 5 is fused image using the method introduced in this paper ($M = 3$, $k = 2$). Visual results show that the spatial information and spectral resolution of the images fused with the method which is clearly improved in this paper.

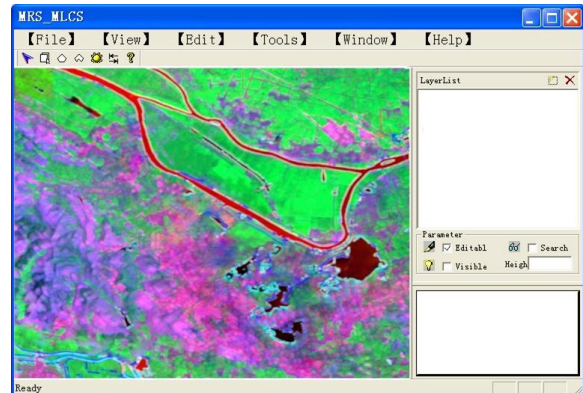


Fig. 2. Original TM image.

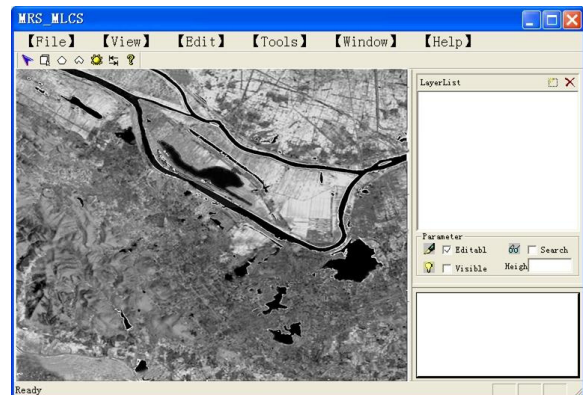


Fig. 3. Original SPOT-PAN image.

In Fig. 4, A1 indicates Erdaohé mine area, A2 indicates Xinzhuangzi mine area, A3 indicates Xie-2 mine area, B1 indicates Lizuizi mining area, B2 indicates Xie-1 mine area. The field investigation shows that most of the disappeared subsidence areas are corresponding to the landfill area, such as Lizuizi mining area (B1) and the area from Xinzhuangzi coal mine to Xie-1 mine (B2), which are all the landfill areas by coal gangue. The large area of newly formed water accumulation areas is corresponding to mining induced subsidence area formed in recent years, such as Erdaohé (A1), Xinzhuangzi mine (A2), and Xie-2 mine (A3).

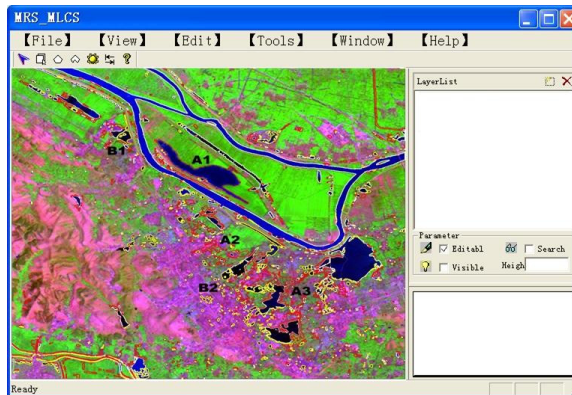


Fig. 4. Fusion image by the method of this paper.

Fig. 5 is the image of Panyi mine in Huainan and Fig. 6 is the Classification of Chaos Immune Algorithm method. The results show that Chaos Immune Algorithm overall accuracy and Kappa coefficient reaches 89.9 % and 0.873 respectively.

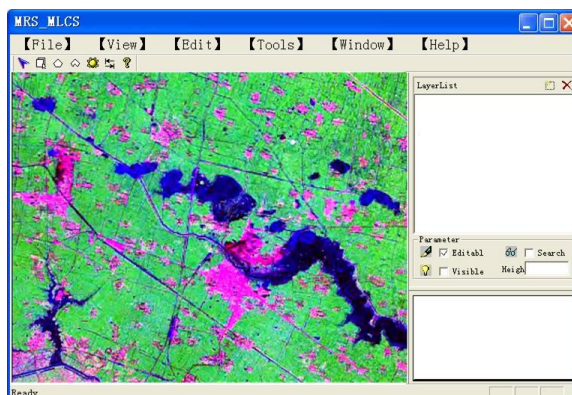


Fig. 5. Image of Panyi mine in Huainan.

Table 1 is matrix of land-use types change in Panji Mine during 2000 to 2004. In this table, the abbreviation for agricultural land is A, the abbreviation for rural construction land is R, the abbreviation for subsidence area is S, the abbreviation for industrial and mineral land is IM, the abbreviation for Water (Huai River and its tributaries) is W. As shown in the

tables, mining subsidence was mainly from cropland. The principle reason is the output of the mine after 2000 rising gradually and maintaining a relatively high efficient level. Since 2000, with the deepening of exploiting degree the original village construction land occur surface settlement, as time appear gradually evolved in to mining subsidence. Worse, lots of cropland occupied because of the village integral transportation, which is the main reason for the relative change rate of construction land transferring to subsidence and cropland transferring to construction land increased.

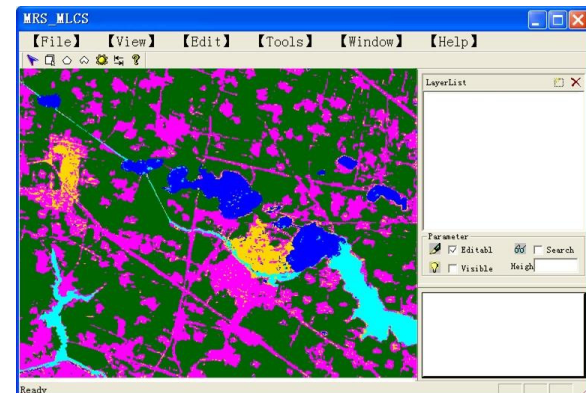


Fig. 6. Classification of CIA method.

Table 1. Matrix of land-use types change in Panji Mine during 2000 to 2004.

Area (hm ²)	A	R	S	IM	W
A	28119.4	655.83	779.17	529.48	0
R	0	14466.26	196.99	148.11	0
S	28.26	0	2096.15	0	0
IM	16.58	0	72.11	7122.03	0
W	52.80	0	63.28	0	4074.66

5. Conclusion

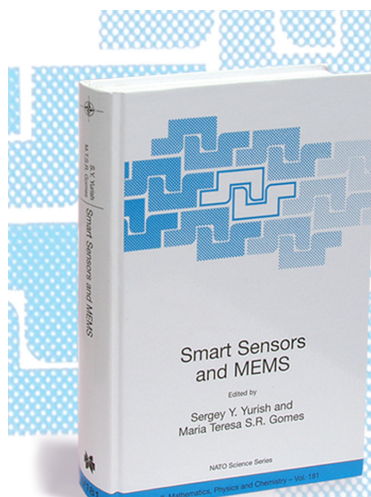
RS monitoring system of land coverage change in mining area is a complex information system. It incorporates RS, GIS technology, land reclamation engineering, land management and virtual reality technology. This paper combined spatial database to store multi-source data of coverage change system, and its core is the remote sensing image fusion and classification.

References

- [1]. G. G. Bhutada, R. S. Anand, S. C. Saxena, Edge preserved image enhancement using adaptive fusion of images denoised by wavelet and cur-velet

- transform, *Digital Signal Processing*, Vol. 21, Issue 1, 2011, pp. 118-130.
- [2]. Biswajeet Pradhan, Amruta Chaudhari, J. Adinarayana, Manfred F. Buchroithner, Soil erosion assessment and its correlation with landslide events using remote sensing data and GIS: a case study at Penang Island, Malaysia, *Environmental Monitoring and Assessment*, Vol. 184, Issue 2, 2012, pp. 715-727.
- [3]. Zheng Liu, E. Blasch, Zhiyun Xue, Objective assessment of multiresolution image fusion algorithms for context enhancement in night vision: a comparative study, *IEEE Transactions on Pattern Analysis and Machine Intelligence*, Vol. 34, Issue 1, 2012, pp. 94-109.
- [4]. A. Ellmauthaler, C. L. Pagliari, E. A. B. da Silva, Multiscale image fusion using the undecimated wavelet transform with spectral factorization and nonorthogonal filter banks, *IEEE Transactions on Image Processing*, Vol. 22, Issue 3, 2013, pp. 1005-1017.
- [5]. Hong Shao, Zhifei Ding, Wencheng Cui, Chest radiographs retrieval based on multi-band wavelet transformation, in *Proceedings of the 2nd International Conference on Information Engineering and Computer Science (ICIECS' 2010)*, Wuhan, China, 25-26 December 2010, pp. 1-4.
- [6]. Nianlong Han, Jinxing Hu, Wei Zhang, Multi-band à trous wavelet transform for multisensor image fusion, in *Proceedings of the 3rd International Congress on Image and Signal Processing (CISP' 2010)*, Yantai, China, 16-18 October 2010, pp. 2207-2211.
- [7]. B. Biswala, M. K. Biswalb, P. K. Dashe, Power quality event characterization using support vector machine and optimization using advanced immune algorithm, *Neurocomputing*, Vol. 103, Issue 1, 2013, pp. 75-86.
- [8]. Qingyang Xu, Song Wang, Li Zhang, A novel chaos danger model immune algorithm, *Communications in Nonlinear Science and Numerical Simulation*, Vol. 18, Issue 11, 2013, pp. 3046-3060.
- [9]. Zheng Qiao Ji, Q. M. Jonathan Wu, An improved artificial immune algorithm with application to multiple sensor systems, *Information Fusion*, Vol. 11, Issue 2, 2010, pp. 174-182.
- [10]. Fafa Chen, Baoping Tang, Renxiang Chen, A novel fault diagnosis model for gearbox based on wavelet support vector machine with immune genetic algorithm, *Measurement*, Vol. 46, Issue 1, 2013, pp. 220-232.

2013 Copyright ©, International Frequency Sensor Association (IFSA). All rights reserved.
(<http://www.sensorsportal.com>)



The book cover features a blue and white geometric pattern on the left side. The title 'Smart Sensors and MEMS' is prominently displayed in the center. Below the title, it says 'Edited by Sergey Y. Yurish and Maria Teresa S.R. Gomes'. At the bottom, it indicates 'NATO Science Series II: Mathematics, Physics and Chemistry - Vol. 151'.

Smart Sensors and MEMS

Edited by
Sergey Y. Yurish and
Maria Teresa S.R. Gomes

The book provides an unique collection of contributions on latest achievements in sensors area and technologies that have made by eleven internationally recognized leading experts ...and gives an excellent opportunity to provide a systematic, in-depth treatment of the new and rapidly developing field of smart sensors and MEMS.

The volume is an excellent guide for practicing engineers, researchers and students interested in this crucial aspect of actual smart sensor design.

Kluwer Academic Publishers

Order online: www.sensorsportal.com/HTML/BOOKSTORE/Smart_Sensors_and_MEMS.htm